ELSEVIER

Thermochimica Acta 244 (1994) 139–151

thermochimica acta

Formation of high surface-area yttrium oxide by the thermal decomposition of different inorganic precursors

Gamal A.M. Hussein

Chemistry Department, Faculty of Science, Minia University, El-Minia 51619, Egypt

Received 17 November 1993; accepted 13 March 1994

Abstract

$Y(CH_3COO)_3 \cdot 4H_2O$, $Y(NO_3)_3 \cdot 5H_2O$ and $Y_2(C_2O_4)_3 \cdot 8H_2O$ were used as precursor compounds for the formation of Y_2O_3 at 100–700°C. Thermal events occurring during the decomposition courses were monitored by means of TG and DTA. Intermediates and final solid products were characterized using infrared spectroscopy and X-ray diffractometry. The Y_2O_3 residues thus formed were subjected to surface and texture investigations. The results indicate that $Y(NO_3)_3 \cdot 5H_2O$ is completely decomposed at 450°C via different unstable intermediates to give high surface area (58 $m^2\ g^{-1}$) Y_2O_3. Both $Y(CH_3COO)_3 \cdot 4H_2O$ and $Y_2(C_2O_4)_3 \cdot 8H_2O$ are completely decomposed at 650°C via $Y_2O_2CO_3$ intermediate. However, $Y(CH_3COO)_3 \cdot 4H_2O$ yields a higher surface-area Y_2O_3 product (55 $m^2\ g^{-1}$) than $Y_2(C_2O_4)_3 \cdot 8H_2O$ (12 $m^2\ g^{-1}$).

Keywords: DTA; IRS; TG; XRD; Yttrium compound; Yttrium oxide

1. Introduction

Cubic-structure yttrium oxide, whose thermal genesis is studied in the present investigation, has numerous applications in various fields. It is an important ingredient in the manufacture of superconductors [1–5] and ceramics [4]. It is also employed as a catalyst [6] and as a support for metal [7] and metal oxide catalysts [8] which have potential applications. The literature has revealed that Kotawski and Lehl [9] studied the thermal decomposition of $Y(CH_3COO)_3 \cdot H_2O$; they reported that dehydration occurs in two steps, at 150 and 220°C. At 350°C the anhydrous acetate decomposes to give $Y_2O_2CO_3$. The latter then decomposes to Y_2O_3 at 630°C.

SSDI 0040-6031(94)01804-P

Patil et al. [10] looked at the decomposition of rare earth nitrates; they stated that the formation of Y_2O_3 takes place via the oxynitrate ($MONO_3$) with a low energy of activation. They also reported that the formation of anhydrous nitrate is possible, in contrast to Wendland and Bear [11] who reported that the anhydrous nitrate is unstable. Also Zaki and Baird [12] studied the decomposition of $(NH_4)_2Ce(NO_3)_6$, and suggested that the decomposition takes place via different intermediates: $(NH_4)HCe(NO_3)_6$ at 150°C, $H_2CeO(NO_3)_4$ at 180°C, and $CeO(NO_3)_2$ at 210°C. At 265°C, CeO_2 is formed. Wendlandt [13] and Moosath et al. [14] studied the thermal decomposition of $Y_2(C_2O_4)_3 \cdot 3H_2O$ and stated that the dihydrate oxalate is stable up to 360°C. Complete dehydration occurs at 400°C, then a rapid decomposition takes place up to 540°C. Finally, Y_2O_3 is formed at 750°C.

It has been established [15] that the composition, structure and surface area of metal oxide catalysts are largely dependent on the method of preparation, the nature of the precursor and the thermal pre-treatment conditions. Accordingly, the present study investigates the thermal genesis pathways of Y_2O_3 from different precursors, namely the acetate, nitrate and oxalate of yttrium, using TG and DTA techniques. The thermal processes revealed were characterized by infrared spectroscopy and X-ray diffractometry.

The Y_2O_3 thus formed from the different precursors were subjected to surface texture assessments, in order to select the best precursor from which and the optimum temperature at which the Y_2O_3 of greatest surface area can be obtained.

2. Experimental

2.1. Yttrium precursors

The $Y(CH_3COO)_3 \cdot 4H_2O$, $Y(NO_3)_3 \cdot 5H_2O$ and $Y_2(C_2O_4)_3 \cdot 8H_2O$ were high purity (99.9%) Aldrich products (USA), abbreviated as YAc, YNit, and YOx, respectively. In view of the thermal analyses results (see below), YAc, YNit and YOx were decomposed by heating at various temperatures (150–800°C) for 1 h in a static air atmosphere. For the sake of simplicity, these products are denoted in the text by YM, where M is Ac or Nit or Ox, followed by the calcination temperature. Thus YNit200 indicates the decomposition products of YNit at 200°C for 1 h. The abbreviation WL stands for weight loss.

2.2. Apparatus and techniques

Thermogravimetry (TG) and differential thermal analysis (DTA) were carried out using a Shimadzu model 30-H (Japan), heating to 700°C at various heating rates ($\theta = 2$, 5, 10 and 20°C min^{-1}) in a flowing air atmosphere (20 ml min^{-1}). The techniques adopted here have been described in detail in a previous paper [16].

Analysis of the solid and gaseous decomposition products of yttrium precursors was performed by means of infrared (IR) and X-ray diffractometry (XRD) using the apparatus and techniques reported earlier [16].

N_2 adsorption isotherms of YAc700, YNit500, YNit700 and YOx700 were determined volumetrically at −195°C using an apparatus based on the design of Lippens [17]. The test samples were pre-outgassed (10^{-6} Torr) (1.33×10^{-5} Pa) at 250°C for 6 h. The surface areas (S_{BET}) were calculated using the BET method [18].

3. Results and discussion

The thermal processes encountered throughout the decomposition course of YAc, YNit and YOx between room temperature and 800°C in flowing air atmosphere (20 ml min^{-1}) are shown in the TG and DTA curves, Fig. 1.

Fig. 2 shows the IR gas-phase spectra over the range 4000–500 cm^{-1}, from the atmosphere surrounding 0.5 g of parent precursor heated to various temperatures (150–600°C) for 5 min.

The IR spectra of the parent precursors and their different calcination products, 150–700°C for 1 h, are given in Fig. 3 and their XRD patterns are shown in Fig. 4.

The N_2 sorption isotherms for YAc700, YNit500, YNit700 and YOx700 are given in Fig. 5. The S_{BET} values computed for YAc700, YNit500, YNit700 and YOx700 are given in Table 1.

3.1. Characterization of the decomposition courses

3.1.1. Yttrium acetate tetrahydrate, $Y(CH_3COO)_3 \cdot 4H_2O$

From the TG and DTA curves (Fig. 1A), it can be seen that process I is an endothermic WL process maximized at 140°C. The WL (21.5%) is very close to that expected (21.3%) for the release of 4 moles of water

$$Y(CH_3COO)_3 \cdot 4H_2O \rightarrow Y(CH_3COO)_3 + 4H_2O \quad (1)$$

In accordance with this, the IR gas-phase spectrum at 250°C (Fig. 2A) displays a broad absorption centred around 3420 cm^{-1} and a strong absorption at 1650 cm^{-1} which are due to the ν(OH) and δ(HOH) vibrations, respectively, of H_2O molecules [19].

The IR spectrum of YAc150 (Fig. 3A) bears a great similarity to that obtained for untreated YAc. It displays bands at 1660, 1560, 1490, 1410, 1360, 1050, 1020, 970, 940, 685 and 620 cm^{-1} which are assignable to the vibration modes of the acetate anion [20,21]. Also the XRD of YAc150 (Fig. 4) displays diffraction lines which are consistent with the existence of anhydrous YAc.

The second step (process II) (Fig. 1A) occurs between 350 and 400°C, causing a 59.8% WL, very close to that expected (60.1%) for the formation of $Y_2O_2CO_3$. This process takes place through three overlapping exothermic peaks. This behaviour suggests that YAc decomposes to $Y_2(CO_3)_3$ (first exothermic peak at 350°C), then to $Y_2O(CO_3)_2$ (second peak at 375°C) and finally to the stable form $Y_2O_2CO_3$ (at 400°C)

$$Y(CH_3COO)_3 \xrightarrow{350°C} Y_2(CO_3)_3 \xrightarrow{375°C} Y_2O(CO_3)_2 \xrightarrow{400°C} Y_2O_2CO_3 \quad (2)$$

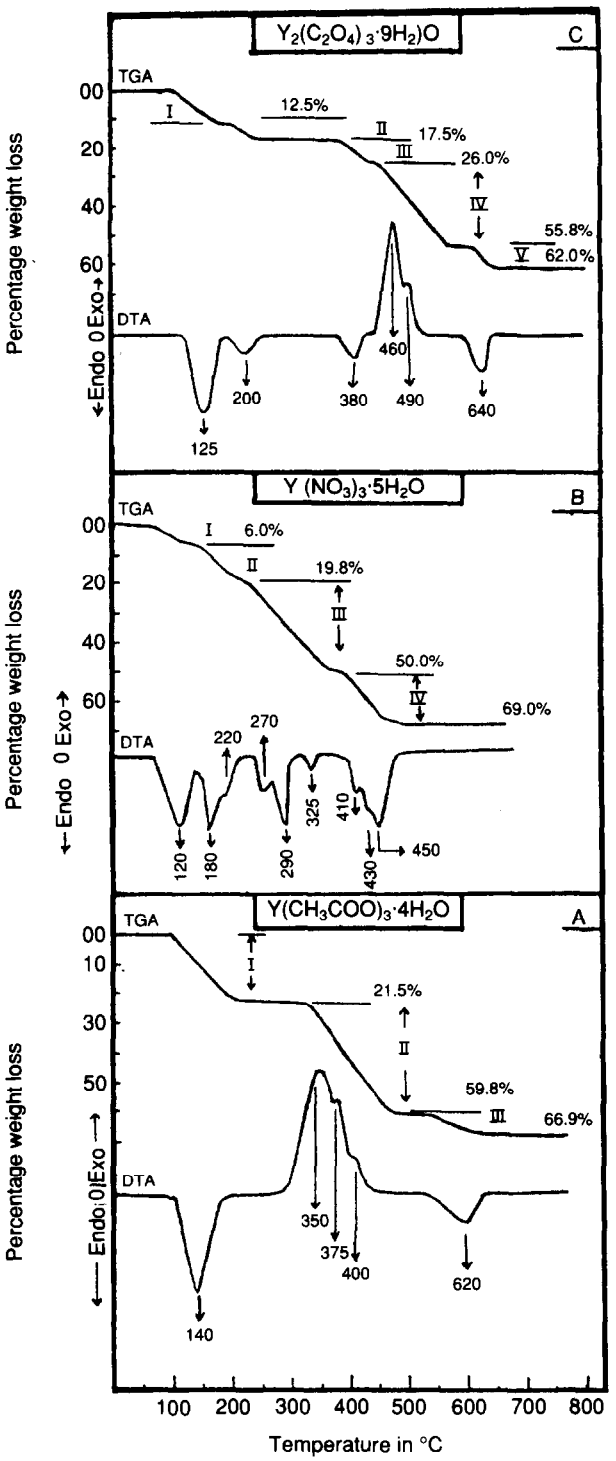

Fig. 1. TG and DTA curves of yttrium oxide precursors.

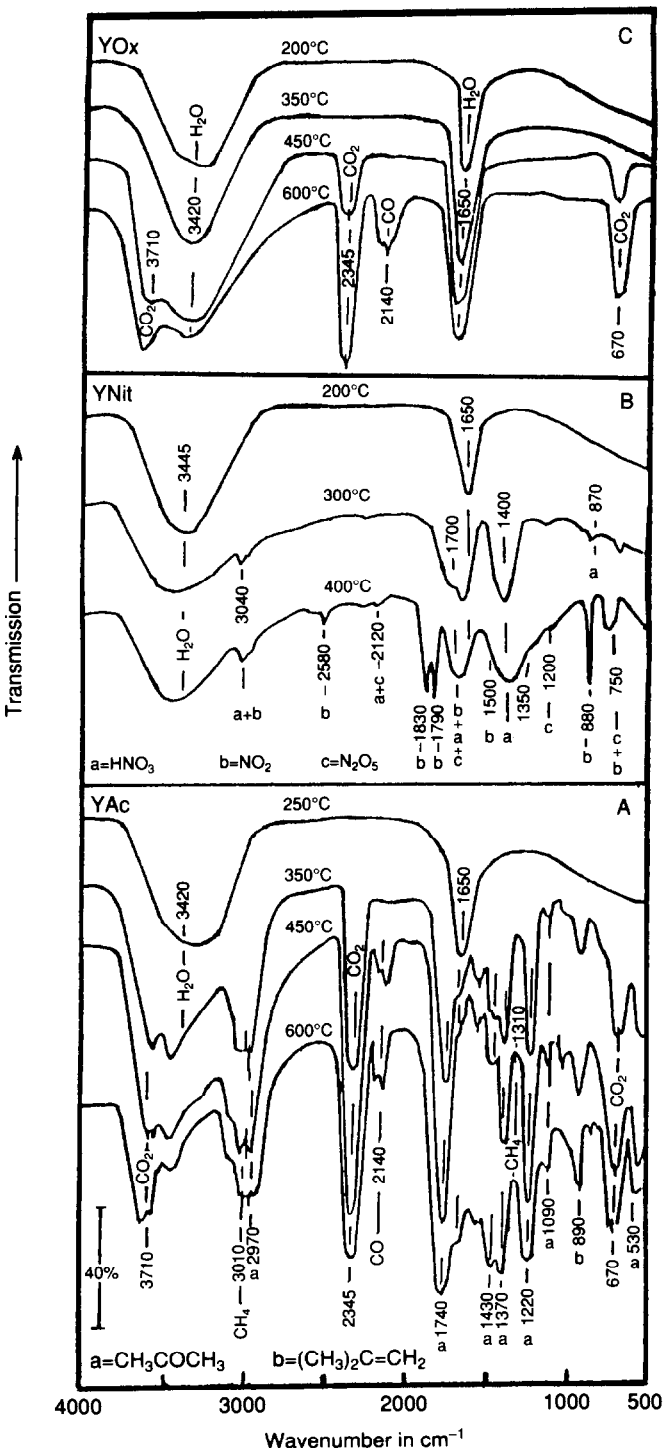

Fig. 2. IR spectra of the gas phase surrounding yttrium oxide precursors heated to various temperatures for 5 min.

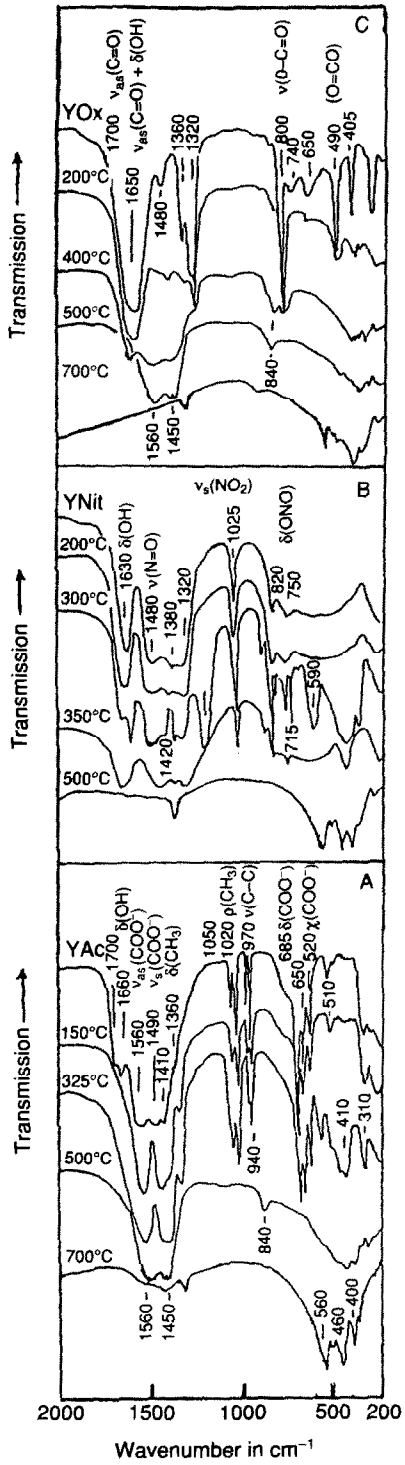

Fig. 3. IR spectra of the yttrium oxide precursors and the products of their heating to various temperatures for 1 h.

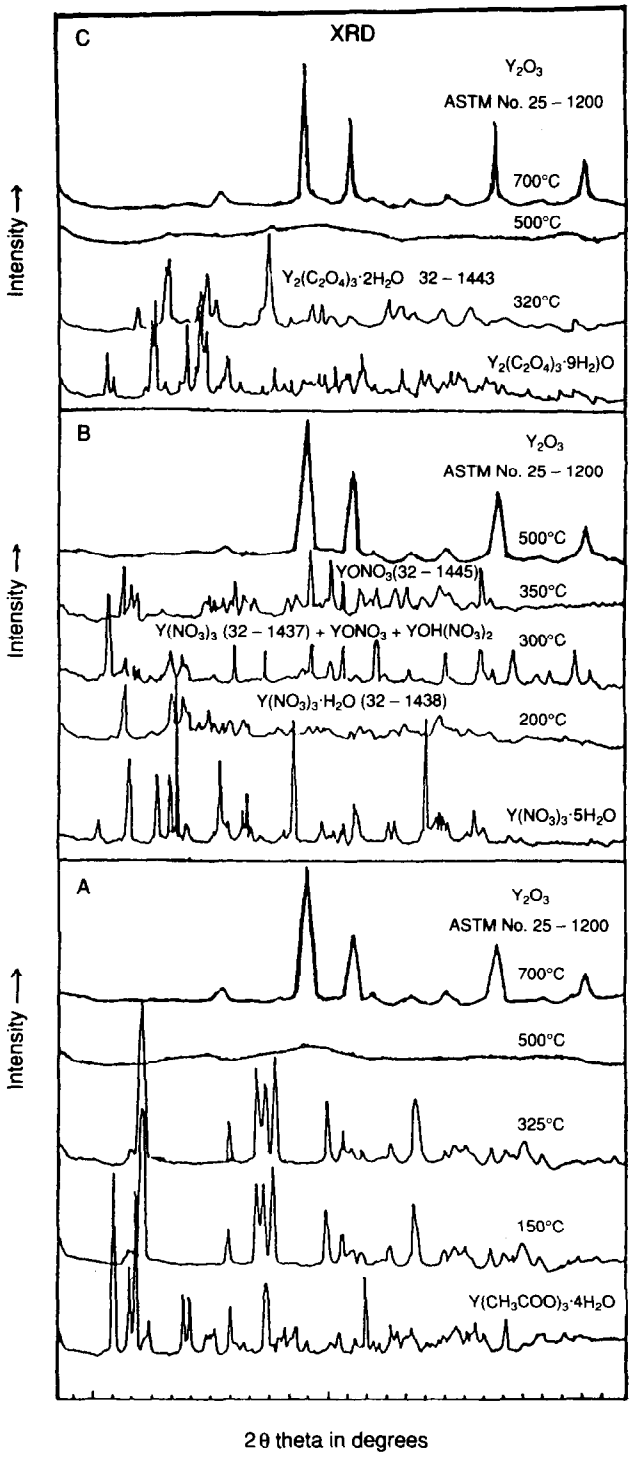

Fig. 4. XRD patterns of the yttrium oxide precursors and the products of their heating to various temperatures for 1 h.

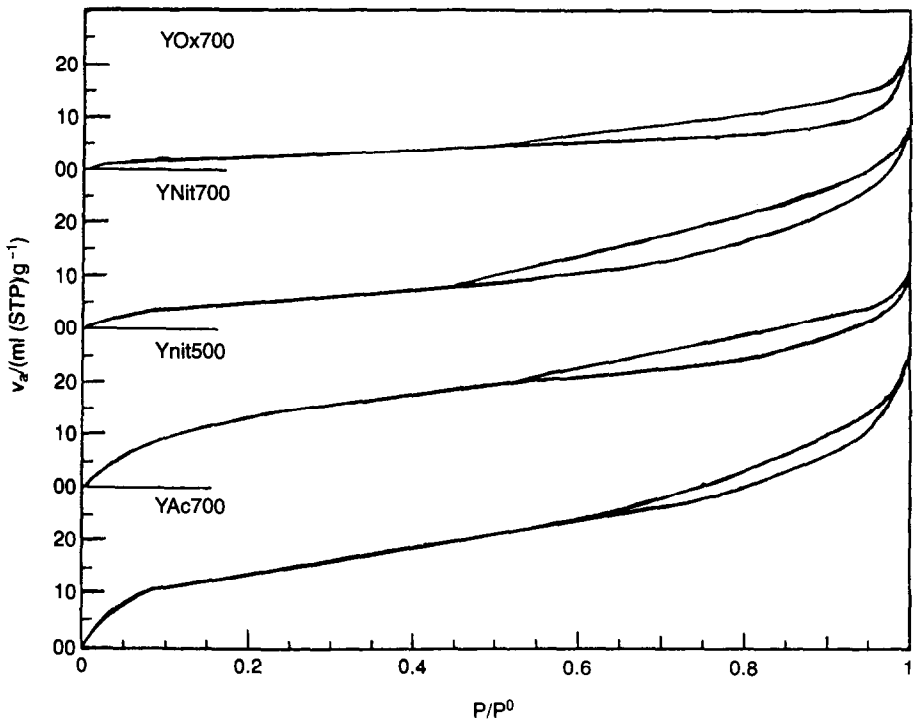

Fig. 5. N_2 sorption isotherms for YAc700, YNit500, YNit700 and YOx700.

Table 1
The S_{BET} values in $m^2\ g^{-1}$ computed for YAc700, YNit500, YNit700 and YOx700

	YAc700	YNit500	YNit700	YOx700
S_{BET}	55	58	20	12

The IR spectra of the gas phase at 350 and 450°C (Fig. 2A) were taken as support for the above results. These spectra display bands due to acetone at 1740, 1430, 1370 and 1220 cm^{-1} [21]. Also, bands due to CO_2 (at 2345 and 670 cm^{-1}) and CO (at 2140 cm^{-1}) are observed. The IR spectrum of YAc500 (Fig. 3A) no longer shows acetate absorption bands, and absorption bands assignable to oxycarbonate species appear at 1560, 1450 and 840 cm^{-1} [22]. Also the strong absorption at 600–300 cm^{-1} is mostly related to Y–O vibration modes [22]. However, the XRD pattern of YAc500 (Fig. 4A) indicates an effective loss of crystal coherency, revealing the predominantly amorphous nature of $Y_2O_2CO_3$.

The third WL step (process III) is endothermic and is maximized at 620°C (Fig. 1A). The total WL (66.9%) is very close to that anticipated (66.6%) for the decomposition of $Y(CH_3COO)_3 \cdot 4H_2O$ to Y_2O_3.

This process involves primarily the decomposition of $Y_2O_2CO_3$ to Y_2O_3. From the IR gas-phase spectrum at 600°C (Fig. 2A), it can be seen that bands due to CO_2 and CO were intensified. Moreover, bands due to CH_4, at 1310 and 3010 cm^{-1}, and isobutene at 890 cm^{-1} are observed. These results were reported previously [15,16,20] and were attributed to the surface bimolecular reaction of acetone, i.e. Y_2O_3 can catalyse the transformation of acetone to isobutene and methane.

The IR spectrum of YAc700 (Fig. 3A) exhibits bands due to Y_2O_3 at 560, 450, 410 and 310 cm^{-1} [22]. In addition the XRD pattern of YAc700 (Fig. 4A) matches that of Y_2O_3 (ASTM No. 25-1200).

3.1.2. Yttrium nitrate pentahydrate, $Y(NO_3)_3 \cdot 5H_2O$

Fig. 1B shows that $Y(NO_3)_3 \cdot 5H_2O$ dehydrates via two endothermic steps maximized at 120 and 220°C. The first WL step of 6% is very close to that expected (6.2%) for release of one mole of water. The second step with a 13.8% WL, i.e. bringing the WL up to 19.8%, is in agreement with the 19.7% corresponding to the release of four moles of water

$$Y(NO_3)_3 \cdot 5H_2O \rightarrow Y(NO_3)_3 \cdot 4H_2O \rightarrow Y(NO_3)_3 \cdot H_2O \quad (3)$$

The DTA curve (Fig. 1B) shows an endothermic effect located near 180°C. A direct visual observation of the physical changes taking place during the decomposition indicates that the material melts at 180°C.

In support, the IR gas-phase spectrum at 200°C (Fig. 2B) shows absorption bands at 3445 and 1650 cm^{-1} due to water molecules [19]. Also the IR spectrum of YNit200 (Fig. 3B) is very similar to that obtained for untreated YNit. It displays absorption bands at 1480, 1380, 1320, 1025, 820, and 750 cm^{-1} due to the nitrate group of a mainly shelving bidentate structure [19]. Moreover, the XRD of YNit200 (Fig. 4B) matches that of $Y(NO_3)_3 \cdot H_2O$ (ASTM No. 32-1438), which reveals that processes I and II correspond to the formation $Y(NO_3)_3 \cdot H_2O$.

Process III (Fig. 1B) takes place through three overlapping endothermic effects located at 270, 290 and 325°C. The total WL determined on completion of this process is 50.0% which is near to that expected (54.2%) for the formation of $YONO_3$

$$Y(NO_3)_3 \cdot H_2O \rightarrow YONO_3 + H_2O + N_2O_5 \quad (4)$$

Reaction (4) is partially corroborated by the IR gas-phase spectrum at 300°C (Fig. 2B) in which characteristic bands due to N_2O_5 (1700, 1350, 1200 and 750 cm^{-1}) [23] and HNO_3 (3040, 1700, 1400 and 870 cm^{-1}) [23] are observed. This indicates that $Y(NO_3)_3 \cdot H_2O$ decomposes simultaneously to give gaseous HNO_3

$$Y(NO_3)_3 \cdot H_2O \rightarrow Y(OH)(NO_3)_2 + HNO_3 \quad (5)$$

Reaction (5) may explain the difference between the determined (50.0%) and calculated (54.2%) WL values.

The IR solid-phase spectrum at 300°C (Fig. 3B) displays bands mainly due to nitrate; the new bands at 1185 and 860 cm^{-1} are due to ν(N=O) (outside the bridge) and ν(N=O) (bridge), respectively [21].

This may suggest the formation of bridging nitro groups. However, the evidence for the formation of oxynitrato anion, $YONO_3$, is quite convincing. The composite strong absorption emerging at 600–300 cm^{-1} is probably related to metal–oxygen-type vibrations (Y–O). Also the band due to δ(OH) (at 1650 cm^{-1}) of $Y(OH)(NO_3)_2$ is still present.

Examining the XRD of YNit300 (Fig. 4B), three different phases are detected: $Y(OH)(NO_3)_2$, $Y(NO_3)_3$ and $YONO_3$. This implies that the product of process III is a multi-component mixture. Therefore it is practically impossible, in the light of these results, to come to any firm conclusions from the TG analysis as to the exact composition of the solid products at 300°C. Nevertheless, the XRD results can confirm that these three products are responsible for the three overlapping endothermic effects (DTA, Fig. 1B).

The TG curve (Fig. 1B) shows that process IV occurs in the temperature range 400–460°C. This process brings the total WL to 69.0%, which is very close to that expected (69.06%) for the decomposition of $Y(NO_3)_3 \cdot 5H_2O$ to Y_2O_3. Thus, process IV involves primarily the decomposition of $Y(NO_3)_3$, $Y(OH)(NO_3)_2$ and $YONO_3$ to Y_2O_3, through the three overlapping endothermic effects located at 410, 430 and 450°C

$$2Y(NO_3)_3 \rightarrow Y_2O_3 + 5NO_2 + N_2O_5 \quad (6)$$

$$2Y(OH)(NO_3)_2 \rightarrow Y_2O_3 + H_2O + 2N_2O_5 \quad (7)$$

$$2YONO_3 \rightarrow Y_2O_3 + N_2O_5 \quad (8)$$

The IR gas-phase spectrum at 400°C (Fig. 2B) displays bands due to HNO_3 and N_2O_5, and new strong absorptions due to NO_2 at 2580, 1830, 1790 and 880 cm^{-1} [21] were also observed.

In support, the solid-phase IR spectrum of YNit500 (Fig. 3B) displays absorption bands due to Y_2O_3 at 560, 460, 400 and 310 cm^{-1} [22]. Also the XRD of YNit500 (Fig. 4B) matches exactly with that of the standard Y_2O_3 (ASTM No. 25-1200).

3.1.3. Yttrium oxalate octahydrate, $Y_2(C_2O_4)_3 \cdot 8H_2O$

The corresponding TG and DTA curves given in Fig. 1C indicate that the reaction decomposition course proceeds through three endothermic stages (I, II and III), which are maximized at 125, 200 and 380°C respectively. The overall WL is 25.0% and has good agreement with that expected (24.6%) for the release of 8 moles of water

$$Y_2(C_2O_4)_3 \cdot 8H_2O \rightarrow Y_2(C_2O_4)_3 \cdot 4H_2O \rightarrow Y_2(C_2O_4)_3 \cdot 2H_2O \rightarrow Y_2(C_2O_4)_3 \quad (9)$$

This result is in good agreement with those of Wendlandt [13] and Moosath et al. [14]. They reported that the oxalates of rare earth metals form stable lower hydrates up to 380°C, and that at temperatures higher than 380°C, dehydration is complete and is followed by rapid decomposition of the oxalates, i.e. the anhydrous oxalate is unstable. This type of process is well characterized by the exothermic behaviour of process IV.

In support, the IR gas-phase spectrum at 200°C (Fig. 2C) displays absorption bands at 3420 and 1650 cm^{-1} due to water molecules [19]; these absorptions intensify further in the 350°C spectrum. Moreover, the IR spectrum of YOx200 (Fig. 3C) is very similar to that obtained for untreated YOx. Also the XRD pattern of YOx200 (Fig. 4C) matches exactly with the standard pattern of $Y_2(C_2O_4)_3 \cdot 2H_2O$ (ASTM No. 32-1443).

Process IV (Fig. 1C) takes place immediately after process III, through two overlapping exothermic processes maximized at 460 and 490°C. The WL monitored by the end of process IV is 55.0%, close to that expected (53.9%) for the formation of $Y_2O_2CO_3$. However, the two exothermic effects may indicate that $Y_2(C_2O_4)_3$ decomposes to $Y_2O_2CO_3$ via an unstable intermediate, probably $Y_2O(CO_3)_2$

$$Y_2(C_2O_4)_3 \rightarrow Y_2O(CO_3)_2 \rightarrow Y_2O_2CO_3 \quad (10)$$

The IR gas-phase spectra at 450 and 600°C (Fig. 2C) display characteristic bands of CO_2 (2345 and 670 cm^{-1}) and CO (2140 cm^{-1}) [21] due to the decomposition of $Y_2(C_2O_4)_3$. One way to support the above results is to analyse the IR spectra of YOx400 at 500°C (Fig. 3C). This analysis indicates the appearance of absorptions assignable to oxycarbonate species (at 1560, 1450 and 840 cm^{-1}) [18], and also the strong absorption emerging at 600–300 cm^{-1} is related to Y–O vibration modes [22]. The XRD of YOx500 (Fig. 4C) indicates a loss in crystallinity (amorphous).

Fig. 1C also indicates that process V takes place endothermally at 640°C, with a WL of 6.1%, which brings the total WL up to 62.0%, close to that expected (61.4%) for the decomposition of $Y_2(C_2O_4)_3 \cdot 8H_2O$ to Y_2O_3.

In corroboration, the IR spectrum of YOx700 (Fig. 3C) lacks oxycarbonate absorption bands. Only bands due to Y_2O_3 are observed. Also the XRD of YOx700 (Fig. 4C) indicates only Y_2O_3, which is highly crystalline in comparison to YAc700 (Fig. 4A) or YNit500 (Fig. 4B).

3.2. Surface texture

Fig. 5 shows the adsorption–desorption isotherms of nitrogen at −196°C on the YAc700, YNit500, YNit700 and YOx700 samples. The isotherms of these samples generally belong to type II of the BET classification [24]. All the isotherms exhibit closed (at $P/P^\circ > 0.45$) hysteresis loops that are nearly of type H3. This suggests that the surface pores are slit-shaped [24].

The measured surface areas (S_{BET}) given in Table 1 indicate that Y_2O_3 obtained from the thermal decomposition of the oxalate and nitrate salts at 700°C exhibit low values of S_{BET}, <20 m^2 g^{-1}. These low values may result from the internal surfaces of both being mostly inaccessible to N_2 molecules. They are apparently sintered more effectively during calcination at 700°C (see Fig. 4) than those of YAc700 and YNit500 which have higher surface areas, >50 m^2 g^{-1}.

4. Conclusions

The thermal decomposition of YAc, YNit and YOx in air involves the following pathways

$$Y(CH_3COO)_3 \cdot 4H_2O \xrightarrow{140^\circ C} Y(CH_3COO)_3 \xrightarrow{350^\circ C} Y_2(CO_3)_3 \xrightarrow{375^\circ C}$$

$$Y_2O(CO_3)_2 \xrightarrow{400^\circ C} Y_2O_2CO_3 \xrightarrow{620^\circ C} Y_2O_3$$

$$Y(NO_3)_3 \cdot 5H_2O \xrightarrow{120^\circ C} Y(NO_3)_3 \cdot 4H_2O \xrightarrow{180^\circ C} Y(NO_3)_3 \cdot 4H_2O(\text{melt}) \xrightarrow{220^\circ C}$$

$$Y(NO_3)_3 \cdot H_2O \xrightarrow{270-325^\circ C} [Y(NO_3)_3 + Y(OH)(NO_3)_2] + YONO_3] \xrightarrow{410-450^\circ C} Y_2O_3$$

$$Y_2(C_2O_4)_3 \cdot 8H_2O \xrightarrow{125^\circ C} Y_2(C_2O_4)_3 \cdot 4H_2O \xrightarrow{200^\circ C} Y_2(C_2O_4)_3 \cdot 2H_2O \xrightarrow{380^\circ C}$$

$$Y_2(C_2O_4)_3 \xrightarrow{460^\circ C} Y_2O(CO_3)_2 \xrightarrow{490^\circ C} Y_2O_2CO_3 \xrightarrow{640^\circ C} Y_2O_3$$

The thermal stability of the anhydrous salts falls in the order YAc ≫ YNit ≫ YOx.

Both the acetate and oxalate of yttrium are decomposed via $Y_2O_2CO_3$ as the stable intermediate amorphous phase.

YAc700 and YNit500 have higher surface areas (>50 m^2 g^{-1}) than YNit700 and YOx700 (<20 m^2 g^{-1}).

References

[1] B. Schulte, M. Maul, W. Becker, E.G. Schlosser, S. Elschner, P. Haussler and H. Adrian, Appl. Phys. Lett., 59(7) (1991) 869.
[2] A.D. Berry, R.T. Holm, M. Fatemi and D.K. Gaskill, J. Mater. Res., 5(6) (1990) 1169.
[3] H. Yamane, H. Masumoto, T. Hirari, H. Iwasaki, K. Watanabe, N. Kobayashi, Y. Muto and H. Kurosawa, Appl. Phys. Lett., 53 (1988) 1548.
[4] F. Uchikawa and J.D. Mackenzi, J. Mater. Res., 4 (1989) 787.
[5] A.J. Lendeen and R. Van Hoozen, J. Org. Chem., 32 (1967) 3386.
[6] B.H. Davis, J. Catal., 52 (1978) 176.
[7] H. Arakawa, Techno Japan, 21(11) (1988) 31.
[8] K. Tanabe, T. Sumiyoshi, K. Shibata, T. Kiyoura and J. Kitagawa, Bull. Chem. Soc. Jpn., 47 (1974) 1064.
[9] A. Kotawski and H. Lehl, Z. Anorg. Chem., 199 (1920) 183.
[10] K.C. Patil, R.K. Gosavi and C.N.R. Rao, Inorg. Chem. Acta, 1 (1967) 155.
[11] W.W. Wendlandt and J.L. Bear, J. Inorg. Nucl. Chem., 12 (1960) 276.
[12] M.I. Zaki and T. Baird, Reactivity of Solids, 2 (1986) 107.
[13] W.W. Wendlandt, Anal. Chem., 31 (1959) 408.
[14] S.S. Moosath, J. Abraham and T.V. Swaminathan, Z. Anorg. Chem., 324 (1963) 99.
[15] G.A.M. Hussein, N. Sheppard, M.I. Zaki and R.B. Fahim, J. Chem. Soc. Faraday Trans. 1, 85(7) (1989) 1732.
[16] G.A.M. Hussein, Thermochim. Acta, 186 (1991) 187.
[17] B.C. Lippens, B.G. Linsen and J.H. de-Boer, J. Catal., 3 (1964) 32.

[18] S. Brunauer, P.H. Emmett and E. Teller, J. Am. Chem. Soc., 60 (1938) 309.
[19] K. Nakamoto, Infrared Spectra of Inorganic and Coordination Compounds, J. Wiley, New York, 1970, p. 253.
[20] S.A.A. Mansour, G.A.M. Hussein and M.I. Zaki, Reactivity of Solids, 8 (1990) 197.
[21] R.H. Pierson, A.M. Fletcher and E.St. Clair Gabtz, Anal. Chem., 28 (1956) 1218.
[22] J.A. Goldsmith and S.D. Ross, Spectrochim. Acta Part A, 23 (1967) 1909.
[23] M. Terada and M. Tsuboi, Bull. Chem. Soc. Jpn., 37 (1964) 1080.
[24] S.G. Gregg and K.S.W. Sing, Adsorption, Surface Area, and Porosity, Academic Press, London, 1967, p. 309.